Quantum phases of hard-core bosons in a frustrated honeycomb lattice

2012 New J. Phys. 14 115028

(http://iopscience.iop.org/1367-2630/14/11/115028)

New Journal of Physics
The open access journal for physics

Quantum phases of hard-core bosons in a frustrated honeycomb lattice

C N Varney[1,7], **K Sun**[2], **V Galitski**[3,4] **and M Rigol**[5,6]

[1] Department of Physics, University of Massachusetts, Amherst, MA 01003, USA
[2] Department of Physics, University of Michigan, Ann Arbor, MI 48109, USA
[3] Joint Quantum Institute and Department of Physics, University of Maryland, College Park, MD 20742, USA
[4] Department of Physics, Condensed Matter Theory Center, University of Maryland, College Park, MD 20742, USA
[5] Department of Physics, Georgetown University, Washington, DC 20057, USA
[6] Physics Department, The Pennsylvania State University, 104 Davey Laboratory, University Park, PA 16802, USA
E-mail: varney@physics.umass.edu

New Journal of Physics **14** (2012) 115028 (14pp)
Received 2 April 2012
Published 28 November 2012
Online at http://www.njp.org/
doi:10.1088/1367-2630/14/11/115028

Abstract. Using exact diagonalization calculations, we investigate the ground-state phase diagram of the hard-core Bose–Hubbard–Haldane model on the honeycomb lattice. This allows us to probe the stability of the Bose-metal phase proposed in Varney *et al* (2011 *Phys. Rev. Lett.* **107** 077201), against various changes in the originally studied Hamiltonian.

[7] Author to whom any correspondence should be addressed.

Contents

1. Introduction

In nature we are surrounded with examples of ordered phases at low temperatures—e.g. crystalline solid structures, magnetically ordered materials, superfluid and superconducting states, etc. While it is straightforward to think of these ordered phases melting as the temperature is increased into the familiar classical liquid or gaseous states that are commonplace in every aspect of our lives, it has been a long-standing question as to whether 'quantum melting' at zero temperature can act similarly to thermal effects and prevent ordering. For a quantum spin or boson system, the resulting state of matter is known as a quantum spin liquid [1]. The interest in such a hypothetical spin liquid has remained strong for decades, most prominently due to the discovery of high temperature superconductivity [2, 3].

Of critical importance is whether a two (or higher)-dimensional system can host a quantum spin liquid. At present, there exists a complete classification of quantum orders [4], which divides hypothetical spin liquids into several distinct classes. Some theoretical stability arguments have also been presented showing that there is no fundamental obstacle to the existence of quantum spin liquids [5]. Gapped spin liquid phases have been observed in dimer models [6–8], and also a family of special exactly-solvable toy models were discovered which can support gapped and gapless spin liquid phases [9]. Although these discoveries clearly demonstrated that a spin-liquid phase may appear in two (or higher) dimensions, at least in toy models, whether the same type of exotic phase can appear in a realistic spin system remains unclear.

Very recently, there has been much numerical [10–17] and experimental [18–20] evidence to suggest the existence of gapped spin liquids in models with SU(2) symmetry, but it is still unclear why these simple models can support such exotic phases. Of particular note are the numerical discoveries of a gapped spin liquid in the Heisenberg model on the kagomé lattice [11] and in the Hubbard model on a honeycomb lattice [10]. The existence of the latter is especially surprising and remains under debate [21]. The nature of this phase has been the subject of many works and it has been argued that next-nearest-neighbor exchange coupling is the mechanism responsible for the quantum spin liquid [13, 14, 22, 23]. However, despite a number of numerical investigations into this J_1–J_2 model, there are still open debates on whether the non-magnetic state present in this model is a valence bond solid [24–28] or a quantum spin liquid [12, 15, 16].

Gapless spin liquids, which may have low-lying fermionic spinon excitations that strongly resemble a Fermi-liquid state, have remained more elusive. Because of these excitations and because spin-1/2 models can be mapped onto hard-core boson models, some of these gapless spin liquids are often referred to as a Bose metal (BM) or Bose liquid. The hallmark feature of a BM is the presence of a singularity in momentum space, known as a Bose surface [29–34]. However, unlike a Fermi liquid, where the Fermi wave vector depends solely on the density of the fermions, the Bose wave vector depends on the control parameters of the Hamiltonian and can vary continuously at fixed particle density.

In this paper, we follow up on the proposition of such a putative BM phase in a simple hard-core boson (XY) model on the honeycomb lattice [34], with an analysis of the stability of this phase against various changes in the Hamiltonian studied originally. First, we examine the dependence of the Bose wave vector on a (phase) parameter that makes the model transition between frustrated and non-frustrated regimes. Next, we show that the phase identified as a BM is stable to breaking of time-reversal symmetry and is present in the phase diagram of the hard-core Bose–Hubbard–Haldane (BHH) model, which features (at least) three phase transitions.

The remainder of this paper is structured as follows. In section 2, we define the model Hamiltonian, briefly discuss the Lanczos algorithm, and define the key observables used in this study: the charge-density wave (CDW) structure factor, the ground-state fidelity metric and the condensate fraction. Next, in section 3, we discuss the identifying characteristics of the BM phase in the context of the hard-core boson (XY) model and show how the Bose wave vector evolves as the parameters are varied. In section 4, we discuss the three phase transitions that we can identify in the BHH model: Bose–Einstein condensate (BEC)–CDW, BEC–BM and BM (other phase)–CDW. The main results are summarized in section 5.

2. Model and methods

2.1. Models

The model proposed in [34] to exhibit a BM phase is the spin-1/2 frustrated antiferromagnetic-XY model on the honeycomb lattice

$$H = J_1 \sum_{\langle ij \rangle} (S_i^+ S_j^- + \text{H.c.}) + J_2 \sum_{\langle\langle ij \rangle\rangle} (S_i^+ S_j^- + \text{H.c.}), \tag{1}$$

where $S_i^{\pm}$ is an operator that flips a spin on site i and J_1 (J_2) is the nearest-neighbor (next-nearest-neighbor) spin exchange. In this model, the next-nearest-neighbor coupling introduces frustration as long as $J_2 > 0$ (antiferromagnetism).

The Hamiltonian in (1) maps to a hard-core boson model ($S_i^+ \to b_i^\dagger$, $S_i^- \to b_i$, and $J_i \to t_i$)

$$H = t_1 \sum_{\langle ij \rangle} \left(b_i^\dagger b_j + \text{H.c.} \right) + t_2 \sum_{\langle\langle ij \rangle\rangle} \left(b_i^\dagger b_j + \text{H.c.} \right). \tag{2}$$

Here $b_i^\dagger$ (b_i) is an operator that creates (annihilates) a hard-core boson on site i and t_1 (t_2) is the nearest-neighbor (next-nearest-neighbor) hopping amplitude. This Hamiltonian was shown to feature four phases: a simple BEC (a zero momentum ($\mathbf{k} = 0$) condensate), a BM (a gapless spin liquid) and two fragmented BEC states. The BM was found to be the ground state of this model over the parameter range $0.210(8) \leqslant t_2/t_1 \leqslant 0.356(9)$ [34].

To better understand the stability of the latter phase, we consider a strongly interacting variant of the Haldane model [35], the hard-core BHH Hamiltonian [36]

$$H = t_1 \sum_{\langle ij \rangle} \left(b_i^\dagger b_j + \text{H.c.} \right) + t_2 \sum_{\langle\langle ij \rangle\rangle} \left(b_i^\dagger b_j \mathrm{e}^{\mathrm{i}\phi_{ij}} + \text{H.c.} \right) + V \sum_{\langle ij \rangle} n_i n_j, \tag{3}$$

which reduces to (2) for $\phi_{ij} = 0$ and $V = 0$. Here, V describes a nearest-neighbor repulsion and the next-nearest neighbor hopping term has a complex phase $\phi_{ij} = \pm\phi$, which is positive for particles moving in the counter-clockwise direction around a honeycomb. Note that the Hamiltonian in (3) can be mapped to a modified XXZ-model ($S_i^+ \to b_i^\dagger$, $S_i^- \to b_i$, $n_i \to S_i^z + 1/2$, $t_1 \to J_1$, $t_2 \to J_2$ and $V \to J_z$)

$$H = J_1 \sum_{\langle ij \rangle} \left(S_i^+ S_j^- + \text{H.c.} \right) + J_2 \sum_{\langle\langle ij \rangle\rangle} \left(S_i^+ S_j^- \mathrm{e}^{\mathrm{i}\phi_{ij}} + \text{H.c.} \right) + J_z \sum_{\langle ij \rangle} \left(S_i^z + \frac{1}{2} \right) \left(S_j^z + \frac{1}{2} \right). \tag{4}$$

The complex phase ϕ plays two important roles. Firstly, for $\phi \neq n\pi$, time-reversal symmetry is explicitly broken. Therefore, we can use this control parameter to study the stability of the BM phase against time-reversal symmetry breaking. Secondly, in the spin language, as we increase the value of ϕ from 0 to π, the sign for the next-nearest-neighbor spin–spin interaction is flipped from positive ($\phi = 0$) to negative ($\phi = \pi$), i.e. the next-nearest-neighbor spin exchange changes from antiferromagnetic to ferromagnetic. Since frustration in this model originates from the antiferromagnetic next-nearest-neighbor spin exchange, we can use ϕ to tune the system from a frustrated ($\phi = 0$) to a non-frustrated ($\phi = \pi$) regime, and thus it enables us to explore the role of frustration in stabilizing the BM phase.

In what follows, $t_1 = 1$ sets our unit of energy, and we fix $t_2 = 0.3$ to focus on transitions from the phase identified in [34] as a BM phase. This model has two limiting cases: (i) for $V \to \infty$, the Ising regime, the ground state is a CDW and (ii) for $V = 0$ and $\phi = \pi$, the non-frustrated regime, the ground state is a simple zero-momentum BEC with non-zero superfluid density.

2.2. *Method and measurements*

To determine the properties of the ground state of (3), we utilize a variant of the Lanczos method [37]. This technique provides a simple and unbiased way to determine the exact ground-state wave function for interacting Hamiltonians. One limitation of the original algorithm is that the Lanczos vectors may lose orthogonality, resulting in spurious eigenvalues [38]. Orthogonality can be restored through reorthogonalization [39], which requires storing the Lanczos vectors. The storage needs can then be reduced utilizing a restarting algorithm, and the most successful techniques are the implicitly restarted [40, 41] and the thick-restart Lanczos algorithms [42]. These two methods are equivalent for Hermitian eigenvalue problems, and here we utilize the thick-restart method for its simplicity in implementation.

A generic and unbiased way of determining the location of a quantum phase transition is related to the ground-state fidelity metric, g [36, 43–46]. The fidelity metric is a dimensionless, intensive quantity and is defined as

$$g = \frac{2}{N} \frac{1 - F(\lambda, \delta\lambda)}{(\delta\lambda)^2}, \tag{5}$$

where N is the number of sites and the fidelity $F(\lambda, \delta\lambda)$ is

$$F(\lambda, \delta\lambda) = \langle \Psi_0(\lambda) | \Psi_0(\lambda + \delta\lambda) \rangle, \tag{6}$$

where $\langle \Psi_0(\lambda) \rangle$ is the ground state of $H(\lambda)$, and λ is the control parameter of the Hamiltonian.

For strong repulsive interactions, the ground state of the BHH model is a CDW insulator, where one of the two sublattices is occupied while the other one is empty. This state spontaneously breaks the sixfold rotational symmetry down to threefold but leaves the lattice translational symmetry intact. In addition, because of the diagonal character of the order established, the structure factor that describes this phase is maximal at zero momentum. Thus, we define the CDW structure factor S_{CDW} as

$$S_{\mathrm{CDW}} = \frac{1}{N} \sum_{i,j} \langle (n_i^a - n_i^b)(n_j^a - n_j^b) \rangle, \tag{7}$$

where n_i^a and n_i^b are the number operators on sublattice a and b in the ith unit cell, respectively.

Another possible ordered state is a BEC, where, in our model, bosons can condense into quantum states in which different momenta are populated. According to the Penrose–Onsager criterion [47], the condensate fraction can be computed by diagonalizing the one-particle density matrix $\rho_{ij} = \langle b_i^\dagger b_j \rangle$,

$$f_{\mathrm{c}} = \Lambda_1 / N_{\mathrm{b}}, \tag{8}$$

where Λ_1 is the largest eigenvalue of ρ_{ij} and N_{b} is the total number of bosons. In a BEC, the condensate occupation scales with the total number of bosons as the system size is increased, which is equivalent to stating that ρ_{ij} exhibits off-diagonal long-range order [48]. Consequently, in a simple BEC, $\Lambda_1 \sim O(N_{\mathrm{b}})$ while all other eigenvalues are $O(1)$ [49]. Aside from a simple BEC, the eigenspectrum of the single-particle density matrix can signal fragmentation, where condensation occurs to more than one effective one-particle state [49, 50], and the BM phase. In the former case, some of the largest eigenvalues are $O(N_{\mathrm{b}})$ and could even be degenerate. For the BM, however, all of the eigenvalues of ρ_{ij} are $\sim O(1)$. Thus finite-size scaling of f_{c} can help pinpoint the presence or absence of condensation.

Further understanding of the latter two phases can be gained by calculating the single-particle occupation at different momentum points

$$n(\mathbf{k}) = \langle \alpha_{\mathbf{k}}^\dagger \alpha_{\mathbf{k}} \rangle + \langle \beta_{\mathbf{k}}^\dagger \beta_{\mathbf{k}} \rangle, \tag{9}$$

where $\alpha_{\mathbf{k}} = \sum_{i \in A} \mathrm{e}^{\mathrm{i}\mathbf{k}\cdot\mathbf{r}_i} b_i^\dagger b_i$ and $\beta_{\mathbf{k}} = \sum_{i \in B} \mathrm{e}^{\mathrm{i}\mathbf{k}\cdot\mathbf{r}_i} b_i^\dagger b_i$ are boson annihilation operators at momentum $\mathbf{k}$ for the A and B sublattices, respectively. In order to minimize finite-size effects and fully probe the Brillouin zone we average over 40×40 twisted boundary conditions [51, 52]

$$\langle n(\mathbf{k}) \rangle_{\theta_x, \theta_y} = \oint \mathrm{d}\theta_x \oint \mathrm{d}\theta_y \langle n(\mathbf{k}, \theta_x, \theta_y) \rangle, \tag{10}$$

where θ_α is the flux associated with the twisted boundary condition.

For any finite-size calculation, there are a large number of clusters that one could study, each with slightly different symmetry properties. In this work, we focus solely on clusters that can be described by a parallelogram or 'tilted rectangle'. The clusters used in this study are illustrated in figure 1 and are discussed in more detail in [34, 36].

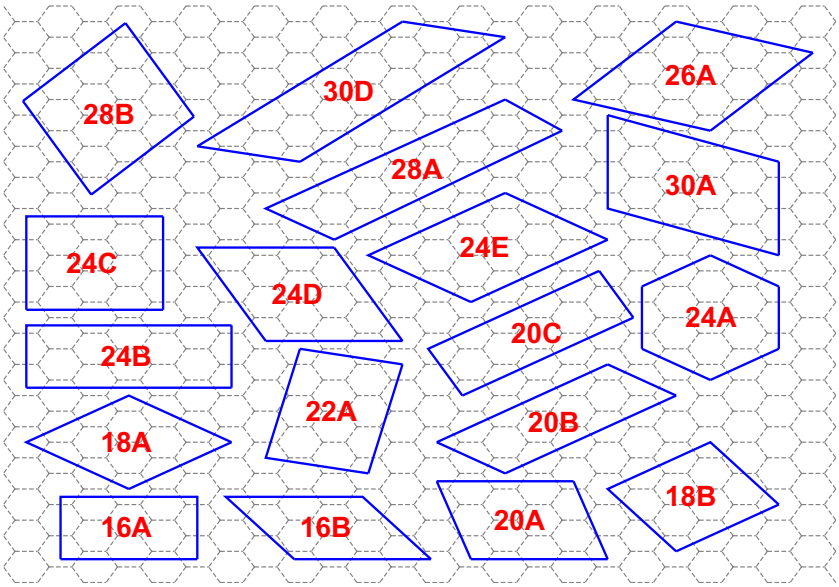

Figure 1. Clusters used in this study.

3. *XY* model

In a previous study [34], we reported that the phase diagram of the XY model (1) on a honeycomb lattice has three quantum phase transitions separating four distinct phases. The four phases are: (i) a BEC $\mathbf{k} = \Gamma$ (antiferromagnetism), (ii) a BM (spin liquid), (iii) a BEC at $\mathbf{k} = M$ (a collinear spin wave) and (iv) a BEC at $\mathbf{k} = K$ (120° order).

The key signature of a BM is the absence of any order and a singularity in the momentum distribution $n(\mathbf{k})$. In figures 2(a) and (b), we show $n(\mathbf{k})$ for two values of t_2/t_1 that are typical for the BM phase. For this phase, $n(\mathbf{k})$ features a t_2/t_1-dependent Bose surface, which, as a guide to the eye, we indicate by a dashed red line. In general, the Bose wave vector q_B at which the maxima of $n(\mathbf{k})$ occurs increases with increasing t_2/t_1, as shown in figure 2(c). We emphasize that the maxima in $n(\mathbf{k})$ do not reflect Bose–Einstein condensation as they do not scale with system size.

4. Bose–Hubbard–Haldane model

In this work, we present evidence that, in the (ϕ, V) plane (see (3)), the BHH model for $t_2/t_1 = 0.3$ exhibits (at least) three phases at half-filling. For strong coupling V, the ground state is a CDW, while (at least) two possible ground states exist at weak-coupling. In the frustrated regime ($\phi \sim 0$) at $V = 0$, the system favors a BM, while the unfrustrated regime ($\phi \sim \pi$) favors a BEC. Consequently, we find that there are three types of transitions: (i) BEC–CDW, (ii) BEC–BM and (iii) BM (other phase)–CDW.

Let us first consider the BEC–CDW transition driven by V at constant ϕ. In figure 3, we show the properties of the system for $\phi = \pi$. In panel (a), we show the fidelity metric versus V, which has a smooth peak that grows with system size, indicative of a second-order phase transition (which would be unconventional in this case in which the system transitions between two ordered states) or a weakly first order transition. If the former is true, the structure

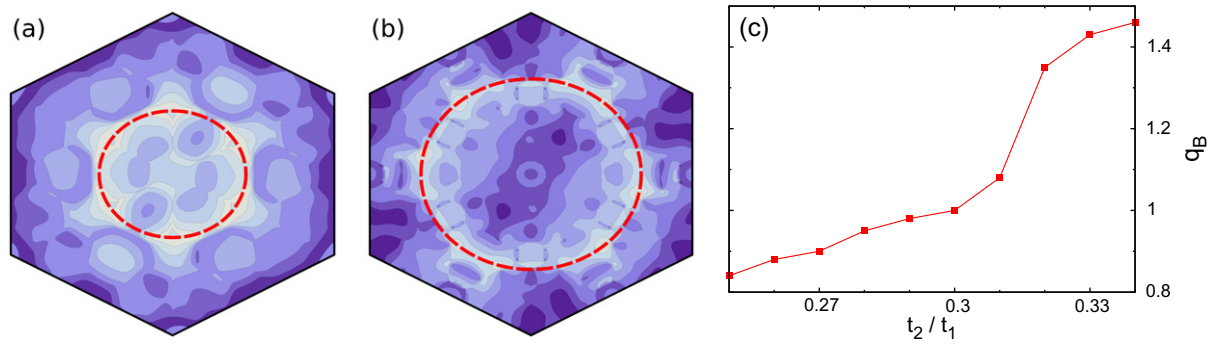

Figure 2. (a), (b) Momentum distribution $n(\mathbf{k})$ versus $\mathbf{k}$[8] for the BM phase in the XY model for $t_2/t_1 = 0.28$ and 0.33, respectively. In both panels, 40×40 twisted boundary conditions were averaged to generate $n(\mathbf{k})$, and the Bose surface is indicated by a dashed red line. (c) The magnitude of the Bose-surface q_B as a function of t_2/t_1.

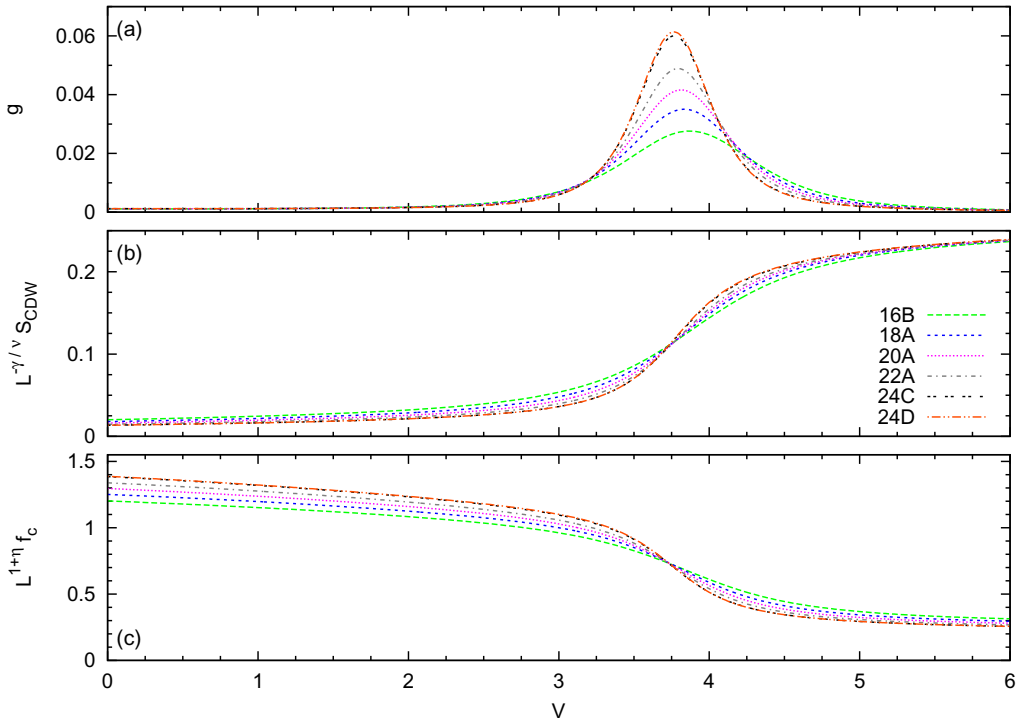

Figure 3. (a) Fidelity metric g, (b) scaled structure factor $L^{-\gamma/\nu} S_{\mathrm{CDW}}$ and (c) scaled condensate fraction $L^{1+\eta} f_c$ as a function of interaction strength for various clusters with $\phi = \pi$.

factor would scale according to the rule

$$L^{-\gamma/\nu} S_{\mathrm{CDW}} = f[(V - V_c) L^{1/\nu}], \tag{11}$$

[8] The momentum distribution $n(\mathbf{k})$ illustrated in figures 2, 5 and 7 were calculated for the $24D$ cluster. All clusters studied here are depicted in figure 1.

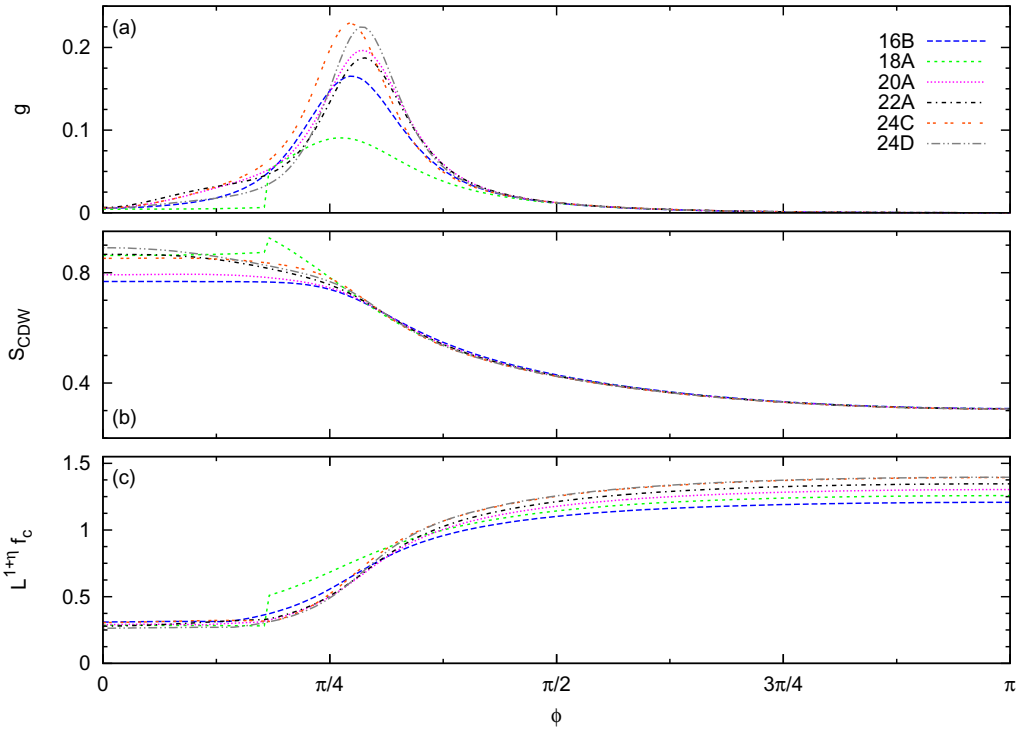

Figure 4. (a) Fidelity metric g, (b) structure factor S_{CDW} and (c) scaled condensate fraction $L^{1+\eta} f_{\mathrm{c}}$ as a function of ϕ for various clusters with $V = 0$.

where N is the number of sites, $L = N^{1/2}$ is the linear dimension and $\gamma = \nu(2-\eta)$. Because of our small lattice sizes, we cannot pinpoint the exact nature of this transition. For example, using a scaling analysis based on the three-dimensional (3D) Ising [53] and XY universality classes [54] yield very similar results. In figure 3(b), we show the CDW structure factor scaled in accordance with the 3D XY universality class, resulting in $V_{\mathrm{c}} = 3.71(7)$.

We can check the robustness of this result by considering the condensate fraction, which scales [55–57] according to

$$L^{y} f_{\mathrm{c}} = g[(V - V_{\mathrm{c}})L^{1/\nu}], \tag{12}$$

where $y = (d + z - 2 + \eta)$. This is illustrated in figure 3(c), resulting in $V_{\mathrm{c}} = 3.73(3)$. This result is quite close to the one obtained using the structure factor. We stress, once again, that although this appears to be a second-order transition between two ordered states, finite-size limitations do not allow us to rule out the possibility of a weak first-order transition or the existence of a small intermediate phase separating the BEC and CDW states.

Next, we examine the properties of the model as one transitions from the BM to the BEC state. In figure 4, we show the same quantities as in figure 3 (this time versus ϕ) for $V = 0$. The fidelity metric is plotted in figure 4(a), and peaks at approximately $\phi \sim 0.88$. In figure 4(b), we show the structure factor, which does not scale with finite size in either phase. Figure 4(c) depicts the scaled condensate fraction, yielding $\phi_{\mathrm{c}} = 0.84 \pm 0.14$, consistent with the peak in the fidelity metric. (Note that the $18A$ cluster experiences a level crossing for $\phi < \phi_{\mathrm{c}}$.) As in the previous case, we cannot make definite statements about the nature of the transition between the BM and the BEC state, but our results are consistent with a second order or a weakly first-order transition.

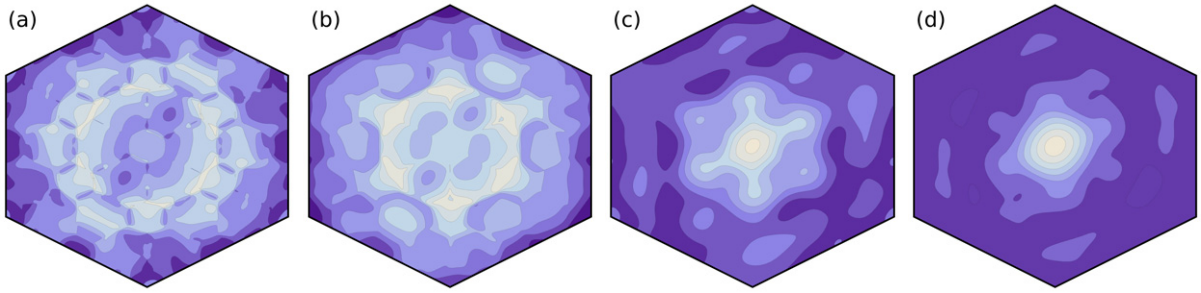

Figure 5. Momentum distribution function $n(\mathbf{k})$ versus $\mathbf{k}$ (see footnote 8) for $V = 0$ and (a) $\phi = 0$, (b) $\phi = \pi/9$, (c) $\phi = \pi/4$ and (d) $\phi = \pi/3$.

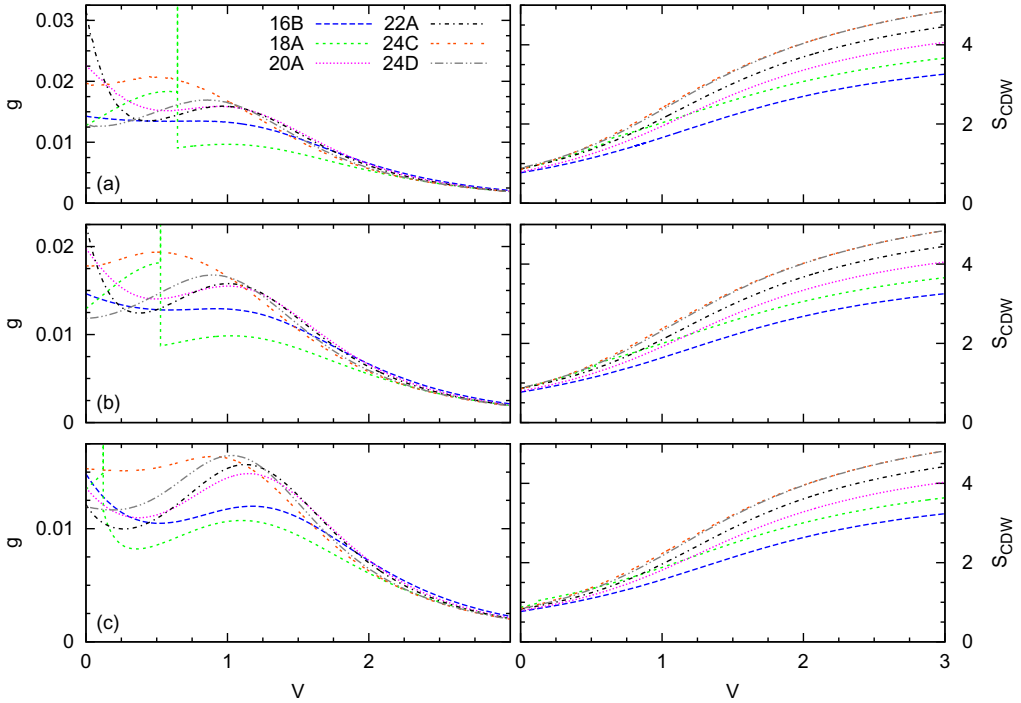

Figure 6. Fidelity metric g (left) and structure factor S_{CDW} (right) as a function of interaction strength for various clusters with (a) $\phi = 0$, (b) $\phi = \pi/12$ and (c) $\phi = \pi/6$.

It is now interesting to study how the Bose surface changes as ϕ increases and one transitions between the BM and the BEC phase. In figure 5, we show the momentum distribution function for four values of ϕ and fixed $V = 0$. As seen in figure 5(b), the Bose surface reduces in size as ϕ departs from zero and continues to shrink until condensation occurs at $\mathbf{k} = \Gamma$ (see figures 5(c) and (d)) for $\phi > \phi_c$.

A third phase transition is expected as V is increased from zero and the BM phase is destroyed to give rise to the large V CDW phase. We illustrate this regime in figure 6 by plotting the fidelity metric (left panels) and CDW structure factor (right panels) for (a) $\phi = 0$, (b) $\pi/12$ and (c) $\pi/6$. In the left panels, for all three values of ϕ, one can see a sort of two-peak structure in the fidelity metric.

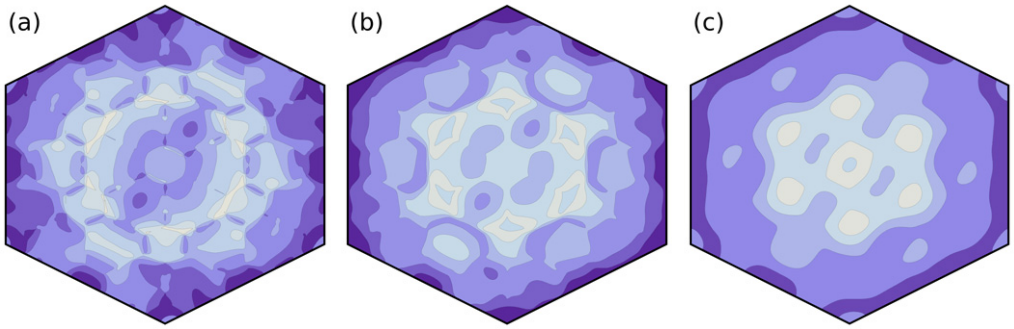

Figure 7. Momentum distribution function $n(\mathbf{k})$ versus $\mathbf{k}$ (see footnote 8) with constant $\phi = 0$ for (a) $V = 0$, (b) $V = 0.25$ and (c) $V = 1$.

The large value of g at $V = 0$ may be an indicator of a transition away from the BM at $V = 0^+$. It is somewhat similar to the behavior of g in both the one-dimensional Hubbard model, where the Mott–metal–insulator phase transition occurs for the onsite repulsion $U = 0^+$ [44], and the two-dimensional hole-doped t–J model [45], where d-wave superconductivity was seen to develop for a superconducting inducing perturbation with vanishing strength. Another possibility is that the BM is stable for positive and small values of V, but a transition to another phase occurs when $V < 0$. The peak produced by such a transition would also explain the structure we see in g. We have also investigated this model with negative values of V, and found that large peaks are present in the fidelity metric for $V < 0$. The position of those peaks had a strong dependence on the cluster geometry. Hence, exactly what happens to the BM phase in the region $V \sim 0$ is something that requires further studies, maybe with other techniques that allow access to larger system sizes and a better finite-size scaling analysis.

For all clusters and values of ϕ depicted in the left panels in figure 6, one can also see a clear peak in the fidelity metric for finite values of V. This feature indicates the onset of CDW order. The structure factor S_{CDW}, depicted in the right panels in figure 6, make apparent that for values of V beyond that peak, the CDW structure factor scales with system size.

In figure 7, we illustrate how the momentum distribution function changes in the presence of interactions at fixed $\phi = 0$. $n(\mathbf{k})$ is shown for $V = 0$ in panel (a) and as the interactions are increased in panels (b) and (c). In figure 7(b), one can see that the Bose-surface broadens as V increases and moves closer to $\mathbf{k} = \Gamma$. Increasing the nearest-neighbor repulsion further, so that the system enters in the CDW phase (figure 7(c)), results in a momentum distribution function that peaked at $\mathbf{k} = \Gamma$, albeit without condensation. Instead, the structure factor $S(\mathbf{k})$ is sharply peaked at $\mathbf{k} = \Gamma$.

A summary of our calculations for different values of V and ϕ is presented in figure 8 as the phase diagram of the hard-core BHH model at half-filling with $t_1 = 1.0$ and $t_2 = 0.3$. For $\phi > \pi/4$, the boundary of the CDW phase was identified by the crossing points in the scaling of the structure factor (figure 3). The boundary of the BEC phase was identified by the crossing points in the scaling of the condensate fraction (figures 3 and 4), and, for small values of V, also using the maximum of the fidelity metric for the largest systems sizes (figure 4). For $\phi < \pi/4$, the CDW transition boundary was determined by the position of the maximum in the peak in the fidelity metric for the largest system sizes (figure 6). Note that, in that regime, the BM phase was found to be stable for $V = 0$. On the other hand, for V between 0 and the boundary of the

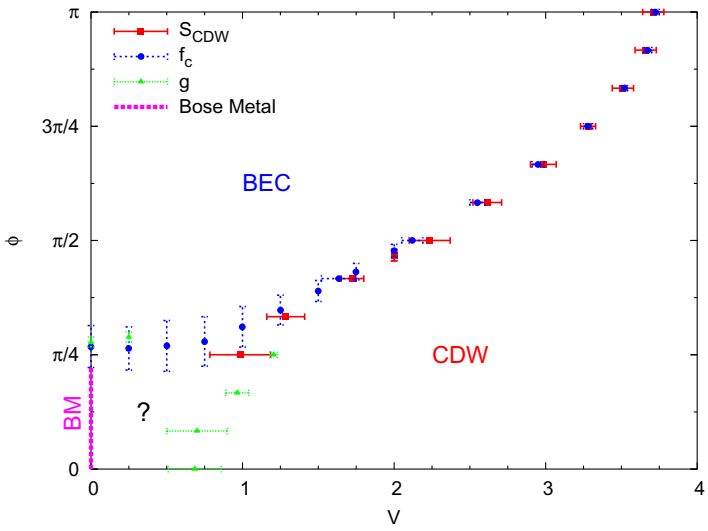

Figure 8. Phase diagram for the BHH model with parameters $t_1 = 1.0$ and $t_2 = 0.3$. The solid red squares are determined by the crossing point in the scaling of S_{CDW}. The solid blue circles are from the crossing point in f_{c}. The green triangles are the average of the location of peak in the fidelity metric for the largest system sizes. The BM phase is indicated by the thick, dashed magenta line.

CDW phase, the large value of the fidelity metric, as well as the behavior of several observables studied in that region, prevent us from making a clear statement about the nature of the ground state.

5. Conclusion

In summary, we have studied the phase diagram of the hard-core BHH Hamiltonian, which has allowed us to probe the effect of perturbations on the BM phase found in the frustrated XY model on a honeycomb lattice [34]. In particular, we explored the parameter dependence of the Bose wave vector and verified that the BM is stable under the effects of time-reversal and chiral symmetry breaking. We identified three phases in the phase diagram of the BHH model: (i) a BM, (ii) a BEC and (iii) a CDW. The phase transitions between the different phases were identified utilizing the ground-state fidelity metric, the CDW structure factor, the condensate fraction and the momentum distribution.

The BEC–CDW transition appears to be second order, although finite-size effects prevent us from ruling out the possibility of a weak first-order transition or the existence of an intermediate phase separating the BEC and the CDW states. If this transition is indeed a direct second-order phase transition, the critical point would be highly non-trivial, and could be an example of deconfined criticality.

We have also found that the BM is destroyed upon increasing V, before the Heisenberg point for nearest-neighbor interactions $V = 2J_1$ can be reached. The presence of a next-nearest-neighbor repulsion may change this and result in transitions to other exotic phases.

Acknowledgments

This research was supported by NSF through JQI-PFC (CNV and KS), ONR (CNV and MR) and US-ARO (VG). The authors thank L Balents, M P A Fisher, T C Lang, and Z Y Meng for useful discussions.

References

[1] Pomeranchuk I Y 1941 *Zh. Eksp. Teor. Fiz.* **11** 226
[2] Anderson P W 1987 The resonating valence bond state in La_2CuO_4 and superconductivity *Science* **235** 1196–8
[3] Lee P A, Nagaosa N and Wen X-G 2006 Doping a Mott insulator: physics of high-temperature superconductivity *Rev. Mod. Phys.* **78** 17–85
[4] Wen X-G 2002 Quantum orders and symmetric spin liquids *Phys. Rev.* B **65** 165113
[5] Hermele M, Senthil T, Fisher M P A, Lee P A, Nagaosa N and Wen X-G 2004 Stability of $U(1)$ spin liquids in two dimensions *Phys. Rev.* B **70** 214437
[6] Rokhsar D S and Kivelson S A 1988 Superconductivity and the quantum hard-core dimer gas *Phys. Rev. Lett.* **61** 2376–9
[7] Moessner R and Sondhi S L 2001 Resonating valence bond phase in the triangular lattice quantum dimer model *Phys. Rev. Lett.* **86** 1881–4
[8] Yao H and Kivelson S A 2012 Exact spin liquid ground states of the quantum dimer model on the square and honeycomb lattices *Phys. Rev. Lett.* **108** 247206
[9] Kitaev A 2006 Anyons in an exactly solved model and beyond *Ann. Phys.* **321** 2–111
[10] Meng Z Y, Lang T C, Wessel S, Assaad F F and Muramatsu A 2010 Quantum spin-liquid emerging in two-dimensional correlated Dirac fermions *Nature* **464** 847
[11] Yan S, Huse D A and White S R 2011 Spin-liquid ground state of the $S = 1/2$ kagomé Heisenberg antiferromagnet *Science* **332** 1173–6
[12] Okumura S, Kawamura H, Okubo T and Motome Y 2010 Novel spin-liquid states in the frustrated Heisenberg antiferromagnet on the honeycomb lattice *J. Phys. Soc. Japan* **79** 114705
[13] Cabra D C, Lamas C A and Rosales H D 2011 Quantum disordered phase on the frustrated honeycomb lattice *Phys. Rev.* B **83** 094506
[14] Clark B K, Abanin D A and Sondhi S L 2011 Nature of the spin liquid state of the Hubbard model on a honeycomb lattice *Phys. Rev. Lett.* **107** 087204
[15] Mezzacapo F and Boninsegni M 2012 Ground-state phase diagram of the quantum J_1–J_2 model on the honeycomb lattice *Phys. Rev.* B **85** 060402
[16] Kalz A, Arlego M, Cabra D, Honecker A and Rossini G 2012 Anisotropic frustrated Heisenberg model on the honeycomb lattice *Phys. Rev.* B **85** 104505
[17] Yang H-Y, Albuquerque A F, Capponi S, Läuchli A M and Schmidt K P 2012 Effective spin couplings in the Mott insulator of the honeycomb lattice Hubbard model arXiv:1207.1072
[18] Vachon M-A, Koutroulakis G, Mitrović V F, Ma O, Marston J B, Reyes A P, Kuhns P, Coldea R and Tylczynski Z 2011 The nature of the low-energy excitations in the short-range-ordered region of Cs_2CuCl_4 as revealed by ^{133}Cs nuclear magnetic resonance *New J. Phys.* **13** 093029
[19] Yan Y J, Li Z Y, Zhang T, Luo X G, Ye G J, Xiang Z J, Cheng P, Zou L J and Chen X H 2012 Magnetic properties of the doped spin- $\frac{1}{2}$ honeycomb-lattice compound $In_3Cu_2VO_9$ *Phys. Rev.* B **85** 085102
[20] Liu D-Y, Guo Y, Zhang X-L, Wang J-L, Zeng Z, Lin H Q and Zou L-J 2012 Strongly correlated electronic states and quasi-two-dimensional antiferromagnetism in honeycomb lattice compound $In_3Cu_2VO_9$ arXiv:1202.1861
[21] Sorella S, Otsuka Y and Yunoki S 2012 Absence of a spin liquid phase in the Hubbard model on the honeycomb lattice arXiv:1207.1783

[22] Wang F 2010 Schwinger boson mean field theories of spin liquid states on a honeycomb lattice: projective symmetry group analysis and critical field theory *Phys. Rev.* B **82** 024419
[23] Lu Y-M and Ran Y 2011 Z_2 spin liquid and chiral antiferromagnetic phase in the Hubbard model on a honeycomb lattice *Phys. Rev.* B **84** 024420
[24] Mulder A, Ganesh R, Capriotti L and Paramekanti A 2010 Spiral order by disorder and lattice nematic order in a frustrated Heisenberg antiferromagnet on the honeycomb lattice *Phys. Rev.* B **81** 214419
[25] Albuquerque A F, Schwandt D, Hetényi B, Capponi S, Mambrini M and Läuchli A M 2011 Phase diagram of a frustrated quantum antiferromagnet on the honeycomb lattice: magnetic order versus valence-bond crystal formation *Phys. Rev.* B **84** 024406
[26] Reuther J, Abanin D A and Thomale R 2011 Magnetic order and paramagnetic phases in the quantum J_1–J_2–J_3 Honeycomb model *Phys. Rev.* B **84** 014417
[27] Oitmaa J and Singh R R P 2011 Phase diagram of the J_1–J_2–J_3 Heisenberg model on the honeycomb lattice: a series expansion study *Phys. Rev.* B **84** 094424
[28] Mosadeq H, Shahbazi F and Jafari S A 2011 Plaquette valence bond ordering in a J_1–J_2 Heisenberg antiferromagnet on a honeycomb lattice *J. Phys.: Condens. Matter* **23** 226006
[29] Motrunich O I and Fisher M P A 2007 d-wave correlated critical Bose liquids in two dimensions *Phys. Rev.* B **75** 235116
[30] Sheng D N, Motrunich O I and Fisher M P A 2009 Spin Bose-metal phase in a spin-1/2 model with ring exchange on a two-leg triangular strip *Phys. Rev.* B **79** 205112
[31] Yang H-Y, Läuchli A M, Mila F and Schmidt K P 2010 Effective spin model for the spin-liquid phase of the Hubbard model on the triangular lattice *Phys. Rev. Lett.* **105** 267204
[32] Dang L, Inglis S and Melko R G 2011 Quantum spin liquid in a spin- $\frac{1}{2}$ XY model with four-site exchange on the kagomé lattice *Phys. Rev.* B **84** 132409
[33] Mishmash R V, Block M S, Kaul R K, Sheng D N, Motrunich O I and Fisher M P A 2011 Bose metals and insulators on multileg ladders with ring exchange *Phys. Rev.* B **84** 245127
[34] Varney C N, Sun K, Galitski V and Rigol M 2011 Kaleidoscope of exotic quantum phases in a frustrated XY model *Phys. Rev. Lett.* **107** 077201
[35] Haldane F D M 1988 Model for a quantum hall effect without Landau levels: condensed-matter realization of the 'parity anomaly' *Phys. Rev. Lett.* **61** 2015–8
[36] Varney C N, Sun K, Rigol M and Galitski V 2010 Interaction effects and quantum phase transitions in topological insulators *Phys. Rev.* B **82** 115125
[37] Lanczos C 1950 An iteration method for the solution of the eigenvalue problem of linear differential and integral operators *J. Res. Natl Bur. Stand.* **45** 255
[38] Cullum J K and Willoughby R A 1985 *Lanczos Algorithms for Large Symmetric Eigenvalue Computations: Theory* vol 1 (Boston: Birkäuser)
[39] Simon H D 1984 Analysis of the symmetric Lanczos algorithm with reorthogonalization methods *Linear Algebra Appl.* **61** 101–31
[40] Sorenson D C 1992 Implicit application of polynomial filters in a k-step Arnoldi method *SIAM J. Matrix Anal. Appl.* **13** 357–85
[41] Calvetti D, Raeichel L and Sorenson D 1994 An implicitly restarted Lanczos method for large symmetric eigenvalue problems *Electron. Trans. Numer. Anal.* **2** 1–21
[42] Wu K and Simon H 2000 Thick-restart Lanczos method for large symmetric eigenvalue problems *SIAM J. Matrix Anal. Appl.* **22** 602–16
[43] Zanardi P and Paunković N 2006 Ground state overlap and quantum phase transitions *Phys. Rev.* E **74** 031123
[44] Venuti L C, Cozzini M, Buonsante P, Massel F, Bray-Ali N and Zanardi P 2008 Fidelity approach to the Hubbard model *Phys. Rev.* B **78** 115410
[45] Rigol M, Shastry B S and Haas S 2009 Fidelity and superconductivity in two-dimensional t–J models *Phys. Rev.* B **80** 094529
[46] Gu S-J 2010 Fidelity approach to quantum phase transitions *Int. J. Mod. Phys.* B **24** 4371–458

[47] Penrose O and Onsager L 1956 Bose–Einstein condensation and liquid helium *Phys. Rev.* **104** 576–84
[48] Yang C N 1962 Concept of off-diagonal long-range order and the quantum phases of liquid He and of superconductors *Rev. Mod. Phys.* **34** 694–704
[49] Leggett A J 2001 Bose–Einstein condensation in the alkali gases: some fundamental concepts *Rev. Mod. Phys.* **73** 307–56
[50] Stanescu T D, Anderson B and Galitski V 2008 Spin–orbit coupled Bose–Einstein condensates *Phys. Rev.* A **78** 023616
[51] Poilblanc D 1991 Twisted boundary conditions in cluster calculations of the optical conductivity in two-dimensional lattice models *Phys. Rev.* B **44** 9562–81
[52] Gros C 1992 The boundary condition integration technique: results for the Hubbard model in 1D and 2D *Z. Phys.* B **86** 359–65
[53] Hasenbusch M 2010 Finite size scaling study of lattice models in the three-dimensional Ising universality class *Phys. Rev.* B **82** 174433
[54] Campostrini M, Hasenbusch M, Pelissetto A and Vicari E 2006 Theoretical estimates of the critical exponents of the superfluid transition in ^{4}He by lattice methods *Phys. Rev.* B **74** 144506
[55] Binder K 1981 Finite size scaling analysis of Ising model block distribution functions *Z. Phys.* B **43** 119
[56] Brézin E and Zinn-Justin J 1985 Finite size effects in phase transitions *Nucl. Phys.* B **257** 867
[57] Rath S P and Zwerger W 2010 Full counting statistics of the interference contrast from independent Bose–Einstein condensates *Phys. Rev.* A **82** 053622